Tunable semiconductor slotted lasers for near-infrared Optical Coherence Tomography

Aritra Roy, Saroj K. Patra, and Tomasz Piwonski, *Member, IEEE*

Abstract — The use of Optical Coherence Tomography in the field of clinical diagnosis is significant. There are different types of swept source lasers available on the market today, however, their design and associated complex fabrication process increase their cost. In the work presented here, an economical six-section slotted tunable laser operating near 850 nm has been designed and fabricated using a UV optical lithography process. The laser is monolithically integrable without a need for any regrowth step. Initial characterization has confirmed the high quality of the slot geometry and stable single mode operation within its tuning range.

Index Terms— Optical Coherence Tomography, Ridge waveguide lasers, Semiconductor lasers, Tunable lasers.

I. INTRODUCTION

Optical Coherence Tomography (OCT) is a non-invasive, interferometric technique to capture 2-D or 3-D images of different scattering media. Though primarily OCT is used in clinical diagnosis for examining tissues and organs, it has widespread applications in the inspection of industrial batch production [1,2], semiconductor wafer processing [3], improving the performance of laser welding [4,5] and as well as many others [6,7,8]. In the Global OCT Market Forecast Report 2019-2024 [9], Business Wire predicted that the global OCT market will grow at a rate of 10 -12% annually and it will exceed $1.2 billion in 2024. Presently the market is dominated by Spectral Domain OCT (SD-OCT), but the Swept Source OCT (SS-OCT) is gradually gaining popularity due to its high-speed performance and other advantages [10,11]. In SS-OCT, which uses a spectrally scanning source, the optical frequency is encoded in time. Ideally, the source for an SS-OCT system should offer broadband and continuous tuning range (70-100 nm), high repetition rates (~200 kHz), as well as being able to operate in single mode with a narrow linewidth, high output power (>20 mW) [12] and having a small footprint. Meeting all those requirements is challenging and often requires complex designs. One of the greatest obstacles in large scale implementation of SS-OCT, specifically in portable or handheld OCT devices, is the lack of available economical sources in the market which can be integrated easily with the OCT system [13].

Conventionally swept source semiconductor lasers have been realized using various methods including external cavity, VCSEL, sampled Bragg gratings reflector (SG-DBR), super-structure grating distributed Bragg reflector (SSG-DBR) and surface gratings (slots) [14,15]. Most of these lasers contain movable parts (filters) for tuning their output wavelength [16] which either leads to the occurrence of some instabilities in their operation [17] or require some complex fabrication steps such as the use of e-beam lithography, ultimately increasing their cost. On the other hand, it has been reported that the multi-section slotted lasers operating at 1550 and 1310 nm based on higher order surface etched grating structures [18] can offer similar performance at a reduced fabrication cost due to their simpler process where no regrowth step is required.

Traditionally those devices have been developed for telecommunication applications, however, there is a need for extending their operational wavelength into 800-900 nm range for applications in OCT. Reducing the wavelength allows improving spatial resolution and deeper penetration due to lower absorption in water and hence providing a more detailed image of various tissues and other biological media [19]. Moreover, apart from medical diagnostics, the 800-900 nm range is also suitable for many industrial applications [20]. Finally, the low-cost, high speed and high efficiency silicon detectors can be used for detecting this wavelength range in OCT systems. Despite all the advantages mentioned above, multi-section slotted lasers based on comparable technology are not readily available in the market at 850 nm where many applications of OCT exist [21].

In this work, we present the design and fabrication of the six-section semiconductor slotted laser operating around the central wavelength near 850 nm which utilizes Vernier effect to tune output wavelength. The manuscript is organized as follows. Sec. II describes the design and simulation methodologies for an optimized laser structure. In Sec. III, a low-cost fabrication technique has been presented. Sec. IV addresses the electro-optic characterization of our laser structures. Finally, we summarize our findings in Sec. V followed by references.

II. DESIGN AND SIMULATION

Design parameter optimization is imperative for the realization of stable single mode operation of the laser with a high side mode suppression ratio (SMSR) within the broad tuning range. There are several different parameters related to laser geometry, such as ridge width, slot period and depth, and length of the sections which must be optimized following the properties of the epitaxial structure including gain-bandwidth and refractive index of each layer.

The authors would also like to thank Superlum Inc. for supplying the wafers and Science Foundation Ireland (SFI 17/CDA/4780) for funding this work.

Aritra Roy is with the Tyndall National Institute, University College Cork, Cork, T12R5CP Ireland (e-mail: aritra.roy@tyndall.ie).

Dr. Saroj K. Patra was with the Tyndall National Institute. He is now with IMEC-KU Leuven, Leuven, Belgium (e-mail: sarojkanta.patra@kuleuven.be).

Dr. Tomasz Piwonski is with the Tyndall National Institute, University College Cork, Cork, T12R5CP Ireland (e-mail: tomasz.piwonski@tyndall.ie).

A. *Design of the Laser*

Our design is a ridge waveguide laser that consists of six active sections – i) two Semiconductor Optical Amplifier (SOA) sections, ii) two slotted mirror sections with slightly different slot separations, iii) one gain section and iv) one phase section (cf. Fig. 1a). The epitaxial structure has been acquired from a commercial supplier and it is based on GaAs multiple quantum wells embedded in the AlGaAs barriers. The cross-section view of the entire stack is shown in Fig. 1b.

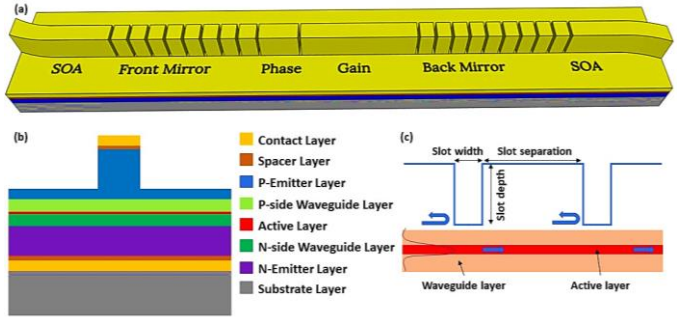

Fig. 1. (a) The proposed design of the six-section swept source laser with slotted mirrors (b) the cross-section view of the ridge depicting all the different layers and (c) the working of the slots in this design.

Both SOA sections act as output power boosters or equalizers depending on the output power requirement of the laser. They can also play the role of a photodetector (PD) if required. Although all the sections provide certain amplification to the optical field inside the laser cavity, the gain section acts as the primary gain control element of the laser. The phase section, which is in principle, a shorter version of the gain section, is used to fine-tune the wavelength of longitudinal modes in the cavity by varying the current dependent refractive index of the section. The wavelength tuning of the laser utilizes the Vernier tuning method [22] which can be implemented by controlling the mirror sections. Each mirror consists of several equally spaced slots (Fig. 1c), which act as higher order surface gratings leading to the creation of reflection peaks at certain wavelengths. The reflectivity peaks also depend on the refractive index of the material. To implement the Vernier effect, the separation between the slots of each mirror is slightly different (Fig. 2d). As a result, just one pair of reflectivity peaks from the two mirrors overlap allowing only that corresponding wavelength [23] to travel back and forth in the optical cavity. The position of each reflectivity peak is controlled independently by changing the current flowing through the mirror sections. Also, to suppress unwanted reflections from the laser facets, both ends of the ridge waveguide are bent at an angle of 7° with respect to the facets with antireflection coatings applied. Additional slots have been incorporated in the design to electrically isolate the adjacent sections of the laser.

B. *Simulation and Optimization*

The optical properties of each section of the laser have been calculated using the commercial simulation software FIMMWAVE/FIMMPROP by Photon Design. These calculations have been performed at the cross-section of the waveguide by solving Maxwell's equation using a finite-difference eigenmode solver (FDM) in the simulation tool. Now, to ensure single transverse mode operation and determine the optimum ridge width and depth, the TE and TM modes have been calculated for GaAs/AlGaAs QW separate confinement heterostructure (SCH). According to our simulation, 2 µm ridge width and 1.7 µm ridge depth guarantee single mode operation thoughout the whole wavelength tuning range with sufficient reflection from the slots (Fig. 2(a, b)). Additionally, we have also verified that the combined thickness of the active and waveguide layer of 0.25 µm ensures a single mode operation in growth direction with an optical confinement factor ($\Gamma_{Transverse}$) of 0.61 [24].

The spectral properties (amplitudes and wavelengths of reflectivity peaks) of the mirror sections have been calculated by using FIMMPROP eigenmode expansion (EME) tool. The tuning range ($\Delta\lambda_{Tuning}$) of the laser depends on the free spectral range (FSR) of both the mirrors, which is the separation between the reflectivity peaks and can be represented by the following formula [25]:

$$\Delta\lambda_{Tuning} = \frac{\Delta\lambda_f \, \Delta\lambda_b}{|\Delta\lambda_f - \Delta\lambda_b|} \quad (1)$$

where, $\Delta\lambda_f$ and $\Delta\lambda_b$ represent the FSR of the front and back mirror respectively which is calculated as follows [23]:

$$\Delta\lambda_{Mirror} = \frac{\lambda_C^2}{2\, d_{Mirror}\, n_{eff}} \quad (2)$$

where, λ_C is the central wavelength, d_{Mirror} is the separation between the slots of the mirror and n_{eff} is the effective refractive index of the waveguide. The FSR value is inversely proportional to the period of the slotted mirror and needs to be optimized considering the maximum shift of the reflectivity peak versus current and the maximum tuning range adjusted to the gain bandwidth of the material. Moreover, it also affects the side mode suppression ratio (SMSR) of the laser. Reflectivity spectra of different slot geometries of the mirror have been simulated with different slot periods (including width and spacing). Another important parameter related to mirror geometry is the slot depth, as it directly affects the maximum achievable reflection of the mirror section [26]. Figure 2c depicts the exponential relationship between the amounts of reflection from the slots and their depth. To increase the reflectance without compromising the transmission, the whole p-emitter region has been etched leaving only a small residual layer of ~200 nm in the slot region. Finally, the total reflectivity of the mirror and the FWHM of the reflectivity peaks also depend on the number of slots in each mirror section. Increasing the number of slots leads to the increase in total reflection, however, at the expanse of the total device length. Considering the central wavelength of 850 nm, available gain bandwidth of 40 nm and effective refractive index of the slot material as 3.33, several designs have been simulated and among them, the ones with slot periods of 38.75 µm and 36.1 µm (corresponding FSR values of 2.75 nm and 2.95 nm respectively) have been selected for fabrication for the tuning range of 40 nm which matches with the gain bandwidth of the material. As the tuning range of the device is limited to 40 nm by the material gain bandwidth, to achieve the wider tuning range complying with the requirement of a good SS-OCT system, electronic synchronization, and optical coupling of the two slotted lasers will be implemented in our future designs. The gain spectrum of these two multi-section lasers, each with a different epitaxial structure, would overlap partially to cover the whole tuning

range. The width of the slot has been chosen as 1 µm to ensure optical photolithography compatible fabrication process. To achieve stable single mode operation and sufficient optical feedback for laser operation, nine slots have been used in each mirror section. The simulated reflectivity spectrum obtained for both mirrors is shown in Fig. 2d. The overlapped reflectivity peaks (encircled in the figure) indicate the selected lasing wavelength.

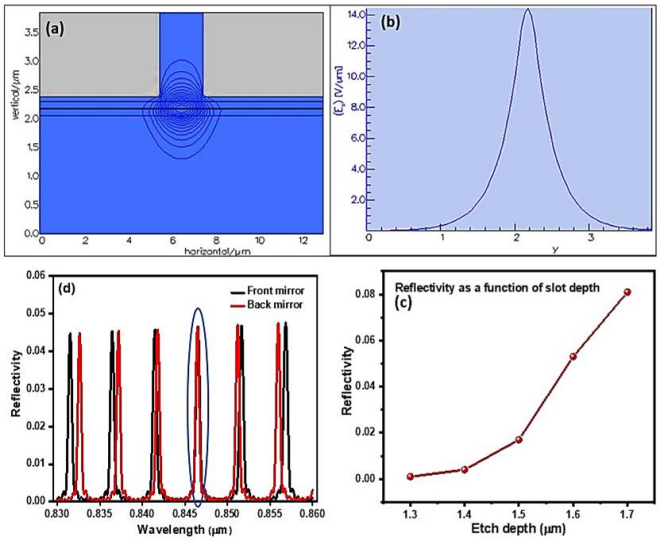

Fig. 2. Simulation of the (a) propagation of the fundamental TE mode and (b) the confinement of the electrical field along the ridge. (c) Dependence of the reflectivity of a slotted mirror with 9 slots on slot depth. (d) The overlapped reflectivity profile of both the front and back mirrors.

Another important parameter for the tunable laser performance is the tuning speed. A-kinetic semiconductor tunable lasers could provide high tuning speed as there are no moving parts. The wavelength sweep could be implemented using a multichannel Arbitrary Waveform Generator (AWG) with V-I converters. Commercially available swept source lasers have been shown to offer tuning speeds up to 200 kHz at different wavelength ranges (1550 and 1310 nm) [27].

III. Fabrication

In order to reduce the complexity, the device fabrication is entirely based on UV lithography and single material dry etch step. It neither requires any re-growth steps nor an expensive and time-consuming e-beam lithography process. All fabrication steps have been optimized to reduce the cost without compromising the performance. A silicon dioxide (SiO_2) hard mask has been created using a very thin resist and vacuum contact to achieve 1 µm resolution. After that, the main pattern has been transferred from the hard mask onto the wafer through dry ICP etching. The etch depth and vertical sidewall profile are among the very critical parameters for laser performance. The recipe, based on BCl_3 – Chlorine, has provided high-quality vertical sidewalls with minimal surface roughness. Also, an optical end-point detection system has been employed for real-time monitoring of the etch depth. The images of the ridge and slot after etching are presented in Fig. 3 (c, d) showing very good smoothness and verticality of the sidewall profiles. After that, SiO_2 has been deposited using PECVD as an isolating layer. To provide current injection, narrow portions of oxide along the ridge have been opened for metal contact deposition. To eliminate the residual reflections from the facets, they were anti-reflection coated using thermal evaporation. The quality of the whole fabrication has been inspected using the scanning electron microscope (SEM) after each step. The whole fabricated device and the SEM images of different sections are presented in Fig. 3.

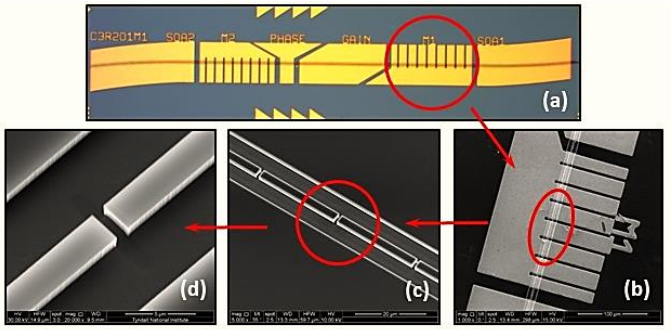

Fig. 3. (a) Fabricated device with all six sections. (b) Zoomed image of the M1 (back mirror) section showing the metal coverage and the ridge. After the material etch, the flat sidewalls of the (c) ridge and (d) slot.

IV. Device Characterization

Initial electro-optic characterization of the cleaved laser chips has been performed using a probe station. Fig. 4 shows the block diagram of the experimental setup.

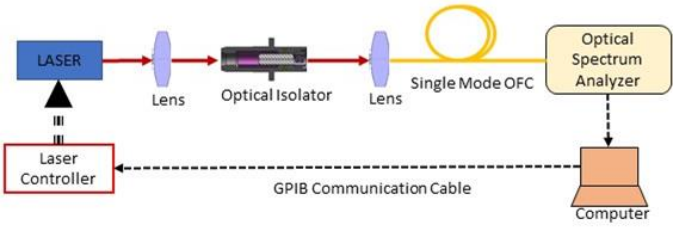

Fig. 4. Block diagram of the experimental set-up for electro-optic characterization of the lasers. The "Laser Controller" refers to 6 independent current sources which separately controls each section of the laser.

The temperature of the laser has been maintained at 20°C using a thermo-electric cooler. Each section of the laser has been driven independently by a dedicated current source. The output emission of the laser has been coupled into a single mode fiber through aspherical lenses and then delivered to an Optical Spectrum Analyzer (OSA). Both laser drivers and the OSA have been controlled by a LabVIEW program.

The current-voltage (I-V) curve of one of the fabricated lasers is shown in Fig. 5(a). The series resistance R_s of ~5Ω is obtained from the gradient of the I-V curve. Together with the electrical isolation of 11kΩ between the sections, the good electrical performance of the devices is confirmed. Also, lasing with a stable single mode operation has been recorded with an SMSR value of 25 dB indicating proper operation of slotted sections (cf. Fig. 5b). The output power of the laser depends on the current combinations applied to different sections of the laser. When the front mirror is pumped with a lower current the crosstalk from the strongly pumped SOA is the largest. To avoid large thermal crosstalk the SOA current is reduced and therefore the output power is lower. Without crosstalk curtailments, the output power is 10 mW. Wavelength tuning of these lasers is realized by varying the front and back mirror currents which change the effective refractive index in turn

leading to the shift of the position of the reflectivity peaks of the mirrors. The initial results of tuning the laser are shown in Fig. 5c. The variation of the output power for the presented device shown in Fig. 5c can easily be adjusted by regulating the SOA drive current of the laser. Both continuous tuning and Vernier tuning has been observed within a small wavelength range (10 nm) due to thermal limitations. These thermal effects are predominant in our setup because of the inefficient heat dissipation from the unmounted laser chips associated with higher drive current for different sections. This restricts the maximum drive current for the mirror sections to 120 mA. These thermal limitations in the laser operation could be circumvented by mounting the laser chip onto a ceramic mount and by placing it in an enclosed butterfly package with a miniaturized thermoelectric cooler (TEC) and heat sink module for efficient heat extraction and dissipation. It can also reduce the thermal crosstalk between the sections. These improvements would substantially aid in enhancing the range of drive current for both the mirror sections and in turn increase the overall tuning range of the device.

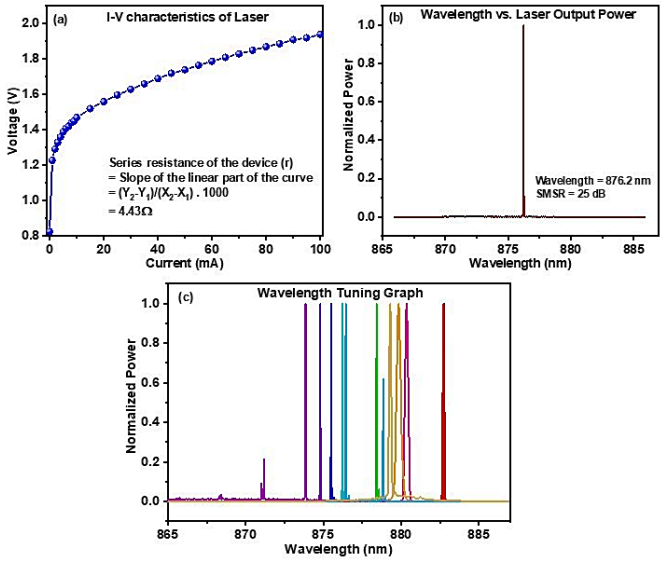

Fig. 5. (a) I-V characteristics of the fabricated laser diode. (b) Laser emission at 876.2 nm. (c) Tuning of the laser with different front and back mirror current combinations.

V. Conclusion

In this work, we have presented simulation, fabrication, and initial electro-optic characterization results of a multi-section semiconductor laser with higher order surface gratings having a central emission wavelength near 850 nm. The laser has exhibited single mode operation with 25 dB of SMSR. Both continuous and Vernier tuning has been observed for a certain wavelength range. The laser performance can be further improved in terms of tuning range and SMSR values by mounting and packaging the laser chips to enhance their thermal performance and further optimization of the design parameters, particularly, the number of slots and their relative depth.

References

[1] T. Tang, C. Zhao, Z. Y. Chen, P. Li, and Z. H. Ding, "Ultrahigh-resolution optical coherence tomography and its application in inspection of industrial materials," *Acta Phys. Sin.*, vol. 64, no. 17, 2015.

[2] D. M. Koller, G. Hannesschläger, M. Leitner, and J. G. Khinast, "Non-destructive analysis of tablet coatings with optical coherence tomography," *Eur. J. Pharm. Sci.*, vol. 44, no. 1–2, pp. 142–148, 2011.

[3] Y. G. Chae, B. Park, M. Kim, Y. Won, and S. Lee, "Imaging for wafer inspection using vertical cavity surface emitting laser based swept source optical coherence tomography," *Opt. InfoBase Conf. Pap.*, vol. F47-D, pp. 2–4, 2017.

[4] C. Stadter, M. Schmoeller, L. von Rhein, and M. F. Zaeh, "Real-time prediction of quality characteristics in laser beam welding using optical coherence tomography and machine learning," *J. Laser Appl.*, vol. 32, no. 2, p. 022046, 2020.

[5] C. Mittelstädt, T. Mattulat, T. Seefeld, and M. Kogel-Hollacher, "Novel approach for weld depth determination using optical coherence tomography measurement in laser deep penetration welding of aluminum and steel," *J. Laser Appl.*, vol. 31, no. 2, p. 022007, 2019.

[6] H. M. Subhash, J. N. Hogan, and M. J. Leahy, "Multiple-reference optical coherence tomography for smartphone applications," *SPIE Newsroom*, no. May, 2015.

[7] M. Dufour, "Inspection of hard-to-reach industrial parts using small-diameter probes," *SPIE Newsroom*, pp. 3–4, 2006.

[8] Y. Huang, M. Badar, A. Nitkowski, A. Weinroth, N. Tansu, and C. Zhou, "Wide-field high-speed space-division multiplexing optical coherence tomography using an integrated photonic device," *Biomed. Opt. Express*, vol. 8, no. 8, p. 3856, 2017.

[9] "Optical Coherence Tomography Market Report and Forecast," 2019.

[10] A. J. Tatham, "Clinical Advantages of Swept-Source OCT and New Non-Damaging Laser Treatments," 2014.

[11] S. Kishi, "Impact of swept source optical coherence tomography on ophthalmology," *Taiwan J. Ophthalmol.*, vol. 6, no. 2, pp. 58–68, 2016.

[12] T. P. Butler *et al.*, "Experimental electric field visualisation of multi-mode dynamics in a short cavity swept laser designed for OCT applications," *Opt. Express*, vol. 27, no. 5, p. 7307, 2019.

[13] Cheryl Guttman Krader, "Understanding advantages, limitations of SS-OCT," 2018.

[14] L. A. Coldren, G. A. Fish, Y. Akulova, J. S. Barton, L. Johansson, and C. W. Coldren, "Tunable Semiconductor Lasers: A Tutorial," *J. Light. Technol.*, vol. 22, no. 1, pp. 193–202, 2004.

[15] W. H. Guo *et al.*, "Integrable slotted single-mode lasers," *IEEE Photonics Technol. Lett.*, vol. 24, no. 8, pp. 634–636, 2012.

[16] M. P. Minneman, J. Ensher, M. Crawford, and D. Derickson, "All-semiconductor high-speed akinetic swept-source for OCT," *Opt. InfoBase Conf. Pap.*, vol. 8311, pp. 1–10, 2011.

[17] S. Slepneva, B. O'Shaughnessy, B. Kelleher, S. P. Hegarty, A. G. Vladimirov, and G. Huyet, "Dynamics of fourier domain mode locked lasers," *2017 Conf. Lasers Electro-Optics, CLEO 2017 - Proc.*, vol. 2017-Janua, no. 16, pp. 1–2, 2017.

[18] M. J. Wallace, G. Jain, R. Mckenna, F. Bello, and J. F. Donegan, "Tuning behaviour of slotted vernier widely tunable lasers," *Opt. Express*, vol. 27, no. 12, p. 17122, 2019.

[19] D. D. John, C. B. Burgner, A. E. Cable, J. G. Fujimoto, and V. Jayaraman, "Single-Mode and High-Speed 850nm MEMS-VCSEL," pp. 4–7, 2016.

[20] J. W. Shi, J. C. Yan, J. M. Wun, J. Chen, and Y. J. Yang, "Oxide-relief and Zn-diffusion 850-nm vertical-cavity surface-emitting lasers with extremely low energy-to-data-rate ratios for 40 Gbit/s operations," *IEEE J. Sel. Top. Quantum Electron.*, vol. 19, no. 2, 2013.

[21] V. J. Srinivasan *et al.*, "High-speed, high-resolution optical coherence tomography retinal imaging with a frequency-swept laser at 850 nm," *Opt. Lett.*, vol. 32, no. 4, p. 361, 2007.

[22] J. Buus, M.-C. Amann, and D. J. Blumenthal, *Widely Tunable Monolithic Laser Diodes*. 2010.

[23] Q. Lu, W. H. Guo, D. Byrne, and J. F. Donegan, "Design of slotted single-mode lasers suitable for photonic integration," *IEEE Photonics Technol. Lett.*, vol. 22, no. 11, pp. 787–789, 2010.

[24] A. Roy, S. Patra, and T. Piwonski, "Low-cost semiconductor swept source laser for near-infrared Optical Coherence Tomography," pp. 1–2, 2020.

[25] J.-J. He and D. Liu, "Wavelength switchable semiconductor laser using half-wave V-coupled cavities," *Opt. Express*, vol. 16, no. 6, p. 3896, 2008.

[26] Q. Y. Lu *et al.*, "Analysis of slot characteristics in slotted single-mode semiconductor lasers using the 2-D scattering matrix method," *IEEE Photonics Technol. Lett.*, vol. 18, no. 24, pp. 2605–2607, 2006.

[27] M. Bonesi *et al.*, "Akinetic all-semiconductor programmable swept-source at 1550 nm and 1310 nm with centimeters coherence length," *Opt. Express*, vol. 22, no. 3, p. 2632, 2014.